

EasyInsert: A Data-Efficient and Generalizable Insertion Policy

Guanghe Li^{1,2,3,4} * Junming Zhao^{1,2,3,5} * Shengjie Wang^{1,2,3} Yang Gao^{1,2,3} †

¹Tsinghua University ²Shanghai AI Laboratory ³Shanghai Qi Zhi Institute
⁴Jilin University ⁵Fudan University

<https://easyinsert.github.io>

Abstract:

Insertion task is highly challenging that requires robots to operate with exceptional precision in cluttered environments. Existing methods often have poor generalization capabilities. They typically function in restricted and structured environments, and frequently fail when the plug and socket are far apart, when the scene is densely cluttered, or when handling novel objects. They also rely on strong assumptions such as access to CAD models or a digital twin in simulation. To address this, we propose EasyInsert, a framework which leverages the human intuition that relative pose (delta pose) between plug and socket is sufficient for successful insertion, and employs efficient and automated real-world data collection with minimal human labor to train a generalizable model for relative pose prediction. During execution, EasyInsert follows a coarse-to-fine execution procedure based on predicted delta pose, and successfully performs various insertion tasks. EasyInsert demonstrates strong zero-shot generalization capability for unseen objects in cluttered environments, handling cases with significant initial pose deviations while maintaining high sample efficiency and requiring little human effort. In real-world experiments, with just 5 hours of training data, EasyInsert achieves over 90% success in zero-shot insertion for 13 out of 15 unseen novel objects, including challenging objects like Type-C cables, HDMI cables, and Ethernet cables. Furthermore, with only one human demonstration and 4 minutes of automatically collected data for fine-tuning, it reaches over 90% success rate for all 15 objects.

Keywords: Robot Manipulation, Generalizable Insertion, Efficient Data Collection

1 Introduction

In modern factory assembly processes, workpieces of diverse shapes require precise assembly. To improve efficiency and achieve automation, some factories employ robots to replace human workers. However, conventional robotic assembly relies on deterministic control programs, necessitating extensive costs for customization. As a result, the pursuit of generalizable robotic assembly solutions has long garnered significant attention. In this work, we focus on insertion—a fundamental yet challenging skill in robotic assembly, characterized by contact-rich manipulation and high precision demands, placing higher demands on robot generalization.

Recent advances in imitation learning, reinforcement learning, and sim-to-real transfer have enabled robots to demonstrate robust performance across increasingly complex assembly tasks. Prior studies often import CAD models of specific workpieces into physics simulators, training agents via

*Equal Contribution

†Corresponding at: gaoyangjiis@mail.tsinghua.edu.cn

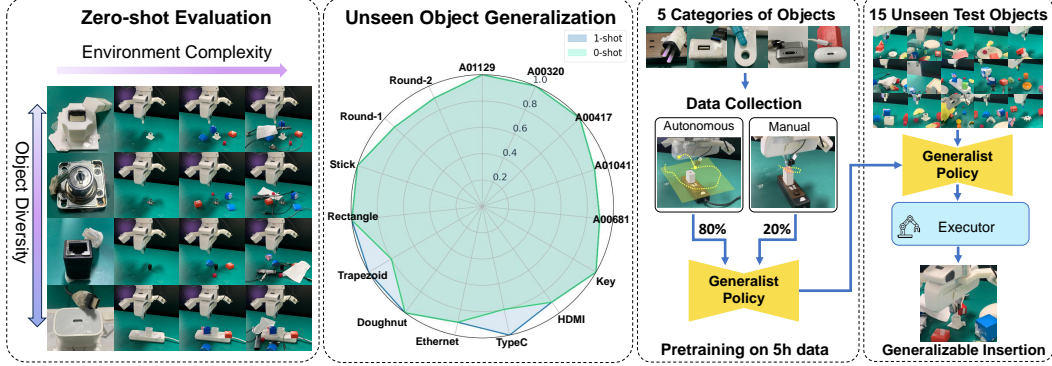


Figure 1: Overview of our framework: (1) Left: Zero-shot evaluation of generalization ability: Along the horizontal axis, the model generalizes to increasingly complex environments starting from a distant initial position. Along the vertical axis, it generalizes to diverse, previously unseen objects. (2) Middle: Generalization performance evaluated under 0-shot and 1-shot settings. (3) Right: Our method’s data collection module gathers 5 hours of pretraining data, with only 20% manually collected. Trained on 5 object categories, the model generalizes to 15 unseen test objects.

reinforcement learning before transferring them to real-world settings [1, 2, 3, 4]. However, these approaches are heavily dependent on accurate CAD models and frequently suffer from performance degradation due to the sim-to-real gap. Moreover, while these works demonstrated their effectiveness on training artifacts, none of them tried to generalize to more unseen objects or diverse environments. Other works tried to overcome the sim2real gap by learning from real-world demonstration [5, 6, 7] or applying RL directly in a real scenario [8, 9, 10]. However, the high cost of collecting real-world data restricts these works to a small and clean environment, fitting models on limited training assembly pairs. In summary, although these prior methods demonstrate competent performance under specific conditions, they fall short in generalizing to more realistic factory scenarios that demand: (1) **Object generalization** – handling previously unseen objects with varied shapes and colors, (2) **Spatial generalization** – adapting to varied initial positions of the objects in a large space, (3) **Environmental generalization** – achieving robust performance across diverse environmental conditions.

In this work, we present **EasyInsert**, an efficient and generalizable framework for robotic insertion tasks. As shown in Figure 1, our generalist policy demonstrates strong generalization across diverse unseen objects, spatial configurations, and environmental conditions—without requiring additional efforts such as CAD model scanning or sim-to-real transfer.

We highlight the importance of sufficient, high-quality real-world data for achieving robust generalization in robotics. While collecting data in the real world is notorious for its high cost, we propose an efficient auto-collecting framework that is both labor-light and scalable. Inspired by how humans perform insertions, we train a visual policy that predicts the delta position and introduce a coarse-to-fine execution strategy based on the prediction. In summary, our contributions include:

1. We propose **EasyInsert**, a framework that efficiently scales real-world training data and achieves strong generalization via delta-pose prediction followed by coarse-to-fine execution, handling unseen objects, diverse spatial configurations, and environmental variations.
2. EasyInsert offers a series of advantages, (1) an automated data collection module that facilitates scalable and high-quality training data with minimal human effort, and (2) a generalist policy that generalizes effectively without requiring additional conditions such as precise CAD models or constrained workspaces. (3) an easy-to-use adaptation finetuning module that automatically collects data and achieves substantial improvements with only one human demonstration.
3. EasyInsert demonstrates remarkable generalization capabilities, achieving over 90% zero-shot success rates across a wide range of unseen objects, spatial positions, and even cluttered

environments. When further enhanced with one-shot fine-tuning, it robustly maintains over 90% success rates on all novel objects.

2 Related Work

We divide previous work on robotic insertion into two categories: Traditional methods and learning based methods.

Traditional Methods for Robotics Insertion. Insertion tasks have long been a focus of research in the robotics community [11]. Traditional approaches to solving insertion problems can be broadly categorized into analytical and heuristic-based methods. Analytical methods [12, 13, 14] rely on geometric, dynamic [15], and mechanical modeling [16], combined with precise sensing, to formulate the insertion problem mathematically and derive solutions through computational analysis. On the other hand, heuristic-based methods [17, 18, 19] employ predefined search patterns tailored to specific objects and robotic systems [20, 21]. These traditional approach typically demand extremely high precision in perception and require extensive manual effort for parameter tuning. Furthermore, their performance is highly susceptible to errors in modeling, sensing, and state estimation, which can significantly degrade robustness in real-world applications.

Learning-based methods for Robotics Insertion. In recent years, learning-based approaches for robotic insertion tasks have gained increasing attention in the robotics community. Several works [1, 2, 3] have developed simulation environments for insertion tasks and demonstrated successful sim-to-real transfer. InsertionNet [6] first performs visual localization before employing local policies for insertion. Zhao et al. [22] utilize offline meta-learning to address insertion tasks, while Nair et al. [23] propose pretraining a reward function and applying reinforcement learning for adaptation to novel objects. SERL [8] tackles insertion through real-world reinforcement learning, and RLIF [24] combines RL with human intervention to solve insertion tasks.

However, these methods typically require precise socket localization (within 1–2 cm accuracy) and a clean workspace—conditions that are often impractical in real-world insertion scenarios. Moreover, they struggle to generalize to unseen objects. In contrast, our method achieves zero-shot insertion for novel objects while tolerating significant initial pose deviations (up to 6 cm in XY translation and 40° in yaw orientation) and operating effectively in cluttered environments.

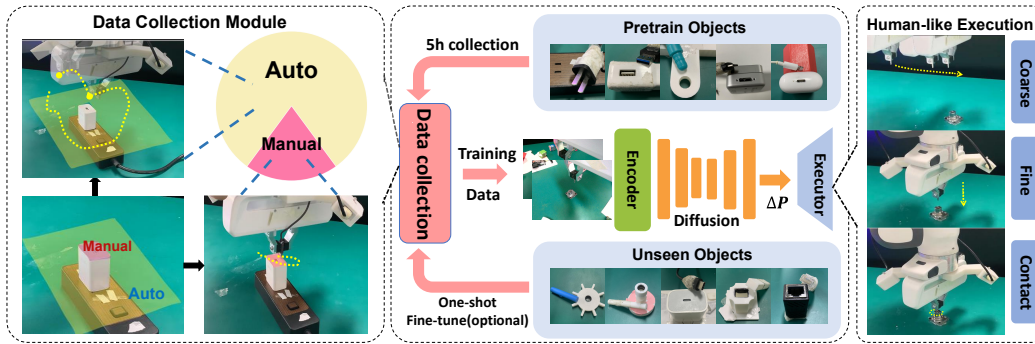


Figure 2: Overview of our method: (1) Left: Data collection module: that constructs training dataset with 80% automated and 20% manual data collection, where manual data collection focuses on fine-grained interactions around the socket area and auto-collection scale data in a larger spatial range. (2) Middle: Generalist Policy pretrained from the collected data, predicts relative pose between plug and socket directly from visual inputs. For tasks requiring higher precision, the same data collection module can be reused to perform one-shot finetuning on the target objects. (3) Right: Motivated by human insertion behavior, we design a similar coarse-to-fine execution process for the robot.

3 Method

Inspired by how humans perform insertion, we designed our framework as 3 parts, shown in Figure 2: (1) **Hybrid dataset construction** that constructs training dataset through automated and manual data collection across 5 categories of objects, (2) **Generalist training** to predict relative pose between plug and socket directly from visual inputs, and (3) **Policy execution** that performs insertion using a coarse-to-fine strategy. When higher accuracy is required for novel test objects, we can fine-tune the generalist model by collecting additional data through our automated data collection module.

3.1 Key Observation

Previous learning-based robotic insertion methods primarily focused on learning to predict precise robot actions or target poses [8, 2, 1]. However, they face significant challenges. In terms of data sources, they require either extensive human teleoperation for imitation, or reinforcement learning with complex reward engineering and real-world interactions [2, 1, 22], which are labor-intensive and time-consuming. Additionally, they may have to make divergent decisions in close proximity regions, complicating the learning process and resulting in poor generalization.

Although humans cannot predict precise actions, they can still perform precise insertion. Initially, they establish approximate alignment between plug and socket at a safe distance. As the plug gets closer, they switch to precise adjustments while gently lowering it. When the plug and socket are in close proximity, humans instinctively use subtle exploratory motions until successful. Throughout this coarse-to-fine insertion process, humans continuously estimate the relative pose (delta-pose) between the plug and socket, which is crucial for precise insertion.

Inspired by this, we propose a novel method that formulates insertion as a delta-pose prediction problem instead of direct action prediction. This approach has two key advantages: (1) Collecting a delta-pose dataset is significantly easier. For every image input, acquiring ground-truth executable robot actions is non-trivial, often requiring human teleoperation or reinforcement learning (RL). In contrast, delta-pose can be computed directly from the gripper’s pose at the insertion point and its current pose. This advantage enables us to develop a semi-automated data collection framework, substantially reducing the burden of manual data acquisition and minimizing human effort. (2) Delta-pose prediction provides a more stable learning objective, maintaining smooth continuity. In contrast, direct action prediction may require highly divergent decisions in close proximity regions, which can compromise generalization performance.

Experiments show that our delta-pose prediction approach achieves over 90% success on most test objects that are unseen during training, highlighting the effectiveness of relative pose estimation in robotic insertion tasks.

3.2 Hybrid Dataset Construction

To train the delta-pose prediction model, we construct a dataset $\mathcal{D} = \{(O_1^i, O_2^i, \Delta \mathbf{p}^i)\}_{i=1}^N$, where O_1^i, O_2^i are images captured by the two wrist-mounted cameras, and $\Delta \mathbf{p}^i$ represents the relative pose transformation from the plug to the socket. We note that following previous works [1, 2, 23, 8], we build our system based on two common assumptions in robotic insertion: (1) The socket maintains a horizontal position on the working surface. (2) The plug’s insertion axis aligns with the gripper’s operational axis in orientation. Consequently, all object poses can be sufficiently characterized by a 4-degree-of-freedom representation: (x, y, z, ψ) , where ψ represents the yaw angle.

We opt to collect data in real-world rather than simulation environments for two key reasons. First, since our method relies on wrist-mounted camera inputs, the significant sim2real gap in RGB imagery would severely degrade performance when transferring learned policies to real-world scenarios. Second, synthetic data often fails to capture the nuanced visual noise and domain variations present in physical environments, making real-world data collection essential for robust performance. Our collected pre-training dataset consists of five categories of paired plugs and sockets, and accumulates of 5 hours of collected data in total as shown in Figure 7. To collect such data, we place the socket

on the table, record gripper pose when plug is inserted into socket, and move the gripper within the workspace around the socket to collect data combining automated and manual strategies. We refer to Appendix A for dataset details, data collection workspace configurations, and how the delta pose is calculated from gripper pose.

Automated Data Collection. The automated data collection module is designed to acquire data efficiently through autonomous, high-speed, and collision-free operations. This is implemented by sampling random poses within the predefined workspace and employing a motion planner to guide the gripper to these target positions at high velocity. During this process, synchronized image pairs and gripper poses $\{(O_1^i, O_2^i, \mathbf{p}^i)\}_{i=1}^N$ are captured at a frequency of 10-15 Hz, which are subsequently converted into training data points. To ensure operational safety and avoid collisions with the socket, when the gripper’s height is detected below a safety threshold, the motion planner immediately executes an upward movement for 2 seconds to maintain safe clearance.

Manual Data Collection. While automated data collection is highly efficient, it fails to capture sufficient data points where the plug and socket are in direct contact. To address this, we manually collect additional data by guiding the Franka arm around the socket to record interactions at near-contact distances. Given the sensitivity of the task, manual operation ensures safer and more controlled data acquisition compared to automated data collection. Notably, this portion of the dataset constitutes only 20% of the total training data. Moreover, since the process only requires physically dragging the Franka arm (without the need for a space mouse), the human effort involved remains minimal.

We note that during automated data collection, a human supervisor introduces environmental variations while the gripper moves by itself. These variations involved randomly rearranging and placing distracting objects near the socket area. This approach effectively generates diverse cluttered environments without requiring the human operator to possess specialized technical knowledge. It is important to note that the supervisor’s involvement was strictly confined to physical workspace modifications, with no requirement for expertise in robotic insertion tasks or system operation.

3.3 Model Training

Pretraining Phase. Given dataset $\mathcal{D} = \{(O_1^i, O_2^i, \Delta \mathbf{p}^i)\}_{i=1}^N$, we adopt Diffusion Policy [25] to train a delta-pose prediction model. For the two images, we use a ResNet18 [26] model pretrained on ImageNet as the shared encoder, and send the fused embedding feature into diffusion action head for delta-pose prediction. Moreover, we utilized DDIM (Denoising Diffusion Implicit Models) as our sampling accelerator, enabling fast real-time inference. Furthermore, to improve the model’s robustness against real-world color variations, we employ strong color augmentation strategies during training, including color jittering and random grayscale conversion. The effectiveness of these augmentation techniques is quantitatively demonstrated through ablation studies in the experimental section. We refer to Appendix B for more details about model pretraining.

One-shot Adaptation. The pretrained delta-pose prediction model has strong generalizability, enabling accurate zero-shot predictions. When higher precision is required, the model can be further fine-tuned on test objects. This process leverages our automated data collection module to obtain approximately 4 minutes of fine-tune data, which is then used to fine-tune the pretrained model. During fine-tuning, we keep the learning rate and other parameters the same as pretraining phase. Importantly, this adaptation phase requires neither manual data collection nor manual environmental variations, as the model’s pretraining on 5h data has already ensured robustness to distractions. The entire adaptation process requires minimal human intervention. Specifically, only a single demonstration needs to be provided manually. After that, the system operates autonomously and fine-tunes itself using only the additional data it collects.

3.4 Policy Execution

Building upon our key observation in Section 3.1, we implement a human-inspired insertion strategy through a coarse-to-fine hierarchical approach based on relative pose prediction. Given the current

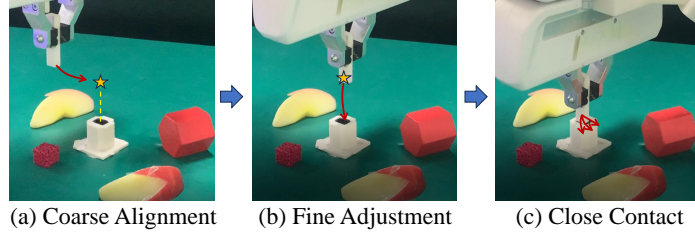


Figure 3: Coarse-to-fine hierarchical insertion procedure.

gripper pose $\mathbf{p} = (x, y, z, \psi)$ and the predicted delta-pose $\Delta\mathbf{p} = (\Delta x, \Delta y, \Delta z, \Delta\psi)$, we estimate the gripper pose at successful insertion as: $\mathbf{p}_g = (g_x, g_y, g_z, g_\psi) = \mathbf{p} + \Delta\mathbf{p}$

Based on \mathbf{p}_g and current gripper pose \mathbf{p} , we compute the next target pose \mathbf{p}_{next} for the gripper and send this to the motion planner, the motion planner will then move a few steps towards \mathbf{p}_{next} .

Coarse Alignment Phase. As shown in Figure 3(a), when the horizontal displacement or angular deviation between the plug and socket exceeds a predefined threshold δ , we send to motion planner a 3D position vertically aligned above \mathbf{p}_g at a safety-critical height H : $\mathbf{p}_{next} = (g_x, g_y, g_z + H, g_\psi)$. Here, we set H as 6 cm.

Fine Adjustment Phase. Once the plug achieves sufficient alignment (i.e., both horizontal and angular deviations fall below δ) as in Figure 3(b), we guide the plug vertically downward toward the socket with high precision: $\mathbf{p}_{next} = (g_x, g_y, z - d_z, g_\psi)$, where we set d_z as 1 cm.

Close-Contact Phase. When the plug and socket are in close proximity as in Figure 3(c), we add random perturbations to accommodate minor misalignments and friction:

$$\mathbf{p}_{next} = (g_x + \beta\epsilon_x, g_y + \beta\epsilon_y, z - d_z, g_\psi), \quad \epsilon_x, \epsilon_y \sim \mathcal{U}(-1, 1), \beta = 3mm \quad (1)$$

The Franka robot executes actions at 15 Hz, querying the diffusion model every 0.5 ~ 1.5 seconds. This hierarchical strategy ensures robust and efficient insertion, balancing high-speed coarse movements with fine adjustments for precision.

4 Experiments

We present a comprehensive evaluation of EasyInsert through 15 real-world insertion tasks, along with ablation studies validating its key design choices.

4.1 Setup

Hardware Setup. The robotic system consists of a 7-DoF Franka Emika Panda arm, using dual wrist-mounted Intel Realsense 405 RGB cameras for visual perception.

Task definitions. We trained EasyInsert on five categories of objects (as illustrated in Figure 10) and evaluated it on 15 novel insertion tasks (shown in Figures 8 and 9). During evaluation, the socket position was randomized within the workspace, while the plug’s initial pose varied with XY-plane offsets of 3–6 cm and yaw angles of 15–40 degrees relative to the socket. To assess environmental robustness, we introduced random distraction objects near the socket, as demonstrated in Figure 4.



Figure 4: Left: We randomly place distraction objects around the socket. Right: In perturbation experiments, we randomly move socket positions.

Table 1: We present here all results. We compare our results with Automate’s performance directly taken from their paper. On Automate objects, EasyInsert achieves average of 96% zero-shot performance, outperforming Automate’s in-domain results of 74%.

Object(AutoMate)	01129	00417	00320	01041	00681
AutoMate	7/10	9/10	10/10	6/10	5/10
EasyInsert	10/10	10/10	10/10	9/10	9/10
Object(Ours)	Key	HDMI	TypeC	Ethernet	Doughnut
EasyInsert	10/10	9/10	8/10	9/10	10/10
Object(Ours)	Trapezoid	Rectangle	Stick	Round-1	Round-2
EasyInsert	8/10	10/10	10/10	9/10	9/10

4.2 Overall Results

Trained on only 5 hours of data, EasyInsert exhibited strong zero-shot generalization across all 15 unseen objects. As shown in Table 1, the method achieved success rates of 90% on most tasks, with only two cases showing lower performance of 80%.

Comparison to baseline. We adopt Automate [1] as our baseline and compare with them across five environments. Automate builds a simulation environment for every insertion object with CAD model and trains a specialist policy. Then, they are distilled into a generalist policy. We directly adopt the in-domain evaluation results reported in their paper, while evaluating our method under a zero-shot setting. Remarkably, tested in a much more cluttered environment and with much greater initial pose deviation, EasyInsert’s zero-shot success rate outperforms AutoMate’s in-domain results [1], highlighting its strong generalization capability.

Object Generalization. Although trained on only five object categories with limited shape variations, EasyInsert exhibited remarkable shape generalization to unseen objects. This capability originates from its efficient data collection that makes good coverage of workspace and delta-pose prediction that only depends on relative pose between plug and socket, which is smooth and consistent across the workspace, making it easy to generalize. The system successfully handles objects divergent from training instances (e.g., HDMI and trapezoidal plugs) and maintains robustness across varying plug-socket color combinations. Notably, as illustrated in Figure 7, round-shaped objects constitute only 7% of the training data, yet the system achieves strong performance on these cases. The observed 80% success rate for Type-C and trapezoidal plugs can likely be attributed to their sockets being very tight, with extremely small tolerances. These objects require higher insertion precision compared to other variants, presenting a more challenging test case for the system’s generalization capabilities.

Spatial Generalization. EasyInsert demonstrates robust spatial generalization capabilities, handling initial pose deviations of up to 6 cm in the xy-plane and 40 degrees in yaw. To further validate its performance under extreme out-of-distribution conditions, we conduct additional rollouts in the HDMI environment with larger perturbations (10 cm offset in XY), achieving a result of 3/5. Notably, even with coarse initial pose estimates in these extreme OOD scenarios, the system effectively guides the gripper towards the socket, performing successful insertions.

Environment Generalization. During evaluation, the presence of distractor objects around the socket did not degrade performance. We attribute this robustness to the manual environmental perturbations during automated data collection, enabling the model to ignore irrelevant features.

Robustness to Perturbation. We conducted additional experiments to evaluate EasyInsert’s robustness against perturbations. During execution, we randomly change the positions of the socket and surrounding distracting objects to test whether EasyInsert could maintain

Object Name	Rectangle	Ethernet	Type-C
EasyInsert	5/5	5/5	4/5

Table 2: Perturbation experiment.

consistent performance. As shown in Table 2, EasyInsert demonstrated stable performance despite the perturbations. This stability is attributed to the closed-loop execution of EasyInsert, which ensures that changes in the positions of distracting objects and the socket do not affect the final outcome.

4.3 One-shot Results

To further improve EasyInsert’s performance, we collected 4 minutes of fine-tune data using the automated data collection module and performed 10 minutes of fine-tuning on a single RTX 3090 GPU. As shown in Table 3, this one-shot adaptation achieved a 100% success rate across all previously failing objects requiring only 30 seconds of human effort and 14 minutes of total runtime including data collection and model fine-tuning.

Object Name	Zero-shot	Fine-tuned
Trapezoid	8/10	10/10
Type-C	8/10	10/10

Table 3: One-shot fine-tuned Performance.

4.4 Ablation Study

In this section, we examine the key designs of EasyInsert across three insertion environments: Type-C, Ethernet, and Stick.

Ablation Study on data augmentation. We investigate the role of data augmentation during pretraining. As shown in Figure 5, removing image augmentations caused a 67% performance drop, particularly for colors that are rare in training data (stick) and transparent objects like Ethernet. This shows the importance of augmentation in bridging domain gaps between training and novel objects.

Ablation Study on manually collected data.

EasyInsert pretrains on both automated and manually collected data. We conduct experiments to examine the necessity of manually collected data. Figure 5 reveals that excluding manually collected data leads to a substantial performance decline. Further analysis of failure cases (detailed in Appendix G) demonstrates that while coarse alignment and fine-adjustment remains successful, the system fails in close-contact phase. This highlights the need for manually-collected close proximity data for achieving precise insertion operations.

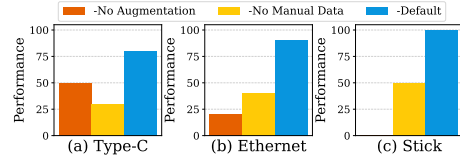


Figure 5: Ablation study on data augmentation and manually collected data.

Ablation Study on Data Amount.

We study the impact of pretraining data amount. Experiment results shown in Figure 6 illustrates that more pretrain data provides better generalization and performance. Notably, trained on 50% of data, EasyInsert maintains 76% zero-shot success rate. However, when the training data is reduced to 12%, the system fails to generalize to novel objects, highlighting the importance of sufficient training samples for robust performance.

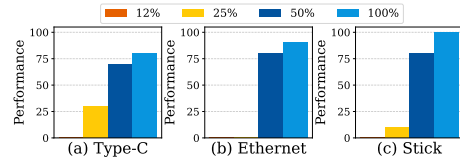


Figure 6: Ablation study on data amount

5 Conclusion

In this paper, we introduce EasyInsert, a novel robotic insertion framework based on human intuition that relative pose between plug and socket is sufficient for insertion, and employs efficient real-world data collection to train an end-to-end model that performs robust insertion using a coarse-to-fine strategy. Extensive experiments demonstrate that EasyInsert achieves remarkable zero-shot success rates on novel objects even in highly cluttered environments with significant initial pose deviation between plug and socket. Furthermore, the system’s performance can be further enhanced through one-shot fine-tuning, showcasing its exceptional generalization capabilities across objects, spatial

configurations, and scenes. We believe this work establishes a robust foundation for advancing general-purpose robotic assembly in industrial applications.

6 Limitation and Future Work

While this study presents promising results, several limitations should be acknowledged. First, our approach assumes an obstacle-free environment between the plug and socket during insertion. In real-world scenarios where obstacles exist, relying solely on delta pose estimation may lead to collisions. To mitigate this limitation, future work could incorporate an obstacle detection module. Such a module could learn to pivot the gripper toward obstacle-free regions before executing delta-pose-based insertion, thereby avoiding collisions. Second, during pretraining data collection, we relied exclusively on real objects rather than incorporating 3D-printed ones, which limited shape diversity in the training dataset. We believe that future work could leverage large-scale 3D-printed objects to construct a more diverse training dataset, leading to a more generalizable insertion policy.

References

- [1] B. Tang, I. Akinola, J. Xu, B. Wen, A. Handa, K. Van Wyk, D. Fox, G. S. Sukhatme, F. Ramos, and Y. Narang. Automate: Specialist and generalist assembly policies over diverse geometries. [arXiv preprint arXiv:2407.08028](#), 2024.
- [2] B. Tang, M. A. Lin, I. Akinola, A. Handa, G. S. Sukhatme, F. Ramos, D. Fox, and Y. Narang. Industreal: Transferring contact-rich assembly tasks from simulation to reality. [arXiv preprint arXiv:2305.17110](#), 2023.
- [3] Y. Narang, K. Storey, I. Akinola, M. Macklin, P. Reist, L. Wawrzyniak, Y. Guo, A. Moravanszky, G. State, M. Lu, et al. Factory: Fast contact for robotic assembly. [arXiv preprint arXiv:2205.03532](#), 2022.
- [4] M. Noseworthy, B. Tang, B. Wen, A. Handa, C. Kessens, N. Roy, D. Fox, F. Ramos, Y. Narang, and I. Akinola. Forge: Force-guided exploration for robust contact-rich manipulation under uncertainty. *IEEE Robotics and Automation Letters*, 2025.
- [5] B. Wen, W. Lian, K. Bekris, and S. Schaal. You only demonstrate once: Category-level manipulation from single visual demonstration. [arXiv preprint arXiv:2201.12716](#), 2022.
- [6] O. Spector, V. Tchuiev, and D. Di Castro. Insertionnet 2.0: Minimal contact multi-step insertion using multimodal multiview sensory input. In *2022 International Conference on Robotics and Automation (ICRA)*, pages 6330–6336. IEEE, 2022.
- [7] K. Yu, Y. Han, Q. Wang, V. Saxena, D. Xu, and Y. Zhao. Mimictouch: Leveraging multi-modal human tactile demonstrations for contact-rich manipulation. [arXiv preprint arXiv:2310.16917](#), 2023.
- [8] J. Luo, Z. Hu, C. Xu, Y. L. Tan, J. Berg, A. Sharma, S. Schaal, C. Finn, A. Gupta, and S. Levine. Serl: A software suite for sample-efficient robotic reinforcement learning. In *2024 IEEE International Conference on Robotics and Automation (ICRA)*, pages 16961–16969. IEEE, 2024.
- [9] J. Luo, C. Xu, J. Wu, and S. Levine. Precise and dexterous robotic manipulation via human-in-the-loop reinforcement learning. [arXiv preprint arXiv:2410.21845](#), 2024.
- [10] C. Xu, Q. Li, J. Luo, and S. Levine. Rldg: Robotic generalist policy distillation via reinforcement learning. [arXiv preprint arXiv:2412.09858](#), 2024.
- [11] D. E. Whitney. *Mechanical assemblies: their design, manufacture, and role in product development*, volume 1. Oxford university press New York, 2004.

- [12] D. E. Whitney. Quasi-static assembly of compliantly supported rigid parts. Journal of Dynamic Systems Measurement and Control-transactions of The Asme, 104:65–77, 1982. URL <https://api.semanticscholar.org/CorpusID:109215697>.
- [13] T. Lozano-Perez, M. T. Mason, and R. H. Taylor. Automatic synthesis of fine-motion strategies for robots. The International Journal of Robotics Research, 3(1):3–24, 1984.
- [14] M. T. Mason. Mechanics of robotic manipulation. MIT press, 2001.
- [15] Y. Xia, Y. Yin, and Z. Chen. Dynamic analysis for peg-in-hole assembly with contact deformation. The International Journal of Advanced Manufacturing Technology, 30:118–128, 2006.
- [16] W. S. Newman, Y. Zhao, and Y.-H. Pao. Interpretation of force and moment signals for compliant peg-in-hole assembly. In Proceedings 2001 ICRA. IEEE International Conference on Robotics and Automation (Cat. No. 01CH37164), volume 1, pages 571–576. IEEE, 2001.
- [17] W. Haskiya, K. Maycock, and J. Knight. Robotic assembly: chamferless peg-hole assembly. Robotica, 17(6):621–634, 1999.
- [18] H. Bruyninckx, S. Dutre, and J. De Schutter. Peg-on-hole: a model based solution to peg and hole alignment. In Proceedings of 1995 IEEE international conference on robotics and automation, volume 2, pages 1919–1924. IEEE, 1995.
- [19] S. R. Chhatpar and M. S. Branicky. Search strategies for peg-in-hole assemblies with position uncertainty. In Proceedings 2001 IEEE/RSJ International Conference on Intelligent Robots and Systems. Expanding the Societal Role of Robotics in the the Next Millennium (Cat. No. 01CH37180), volume 3, pages 1465–1470. IEEE, 2001.
- [20] H. Park, J.-H. Bae, J.-H. Park, M.-H. Baeg, and J. Park. Intuitive peg-in-hole assembly strategy with a compliant manipulator. In IEEE ISR 2013, pages 1–5. IEEE, 2013.
- [21] K. Sharma, V. Shirwalkar, and P. K. Pal. Intelligent and environment-independent peg-in-hole search strategies. In 2013 International Conference on Control, Automation, Robotics and Embedded Systems (CARE), pages 1–6. IEEE, 2013.
- [22] T. Z. Zhao, J. Luo, O. Sushkov, R. Pevceviciute, N. Heess, J. Scholz, S. Schaal, and S. Levine. Offline meta-reinforcement learning for industrial insertion. In 2022 international conference on robotics and automation (ICRA), pages 6386–6393. IEEE, 2022.
- [23] A. Nair, B. Zhu, G. Narayanan, E. Solowjow, and S. Levine. Learning on the job: Self-rewarding offline-to-online finetuning for industrial insertion of novel connectors from vision. In 2023 IEEE International Conference on Robotics and Automation (ICRA), pages 7154–7161. IEEE, 2023.
- [24] J. Luo, P. Dong, Y. Zhai, Y. Ma, and S. Levine. Rlif: Interactive imitation learning as reinforcement learning. arXiv preprint arXiv:2311.12996, 2023.
- [25] C. Chi, Z. Xu, S. Feng, E. Cousineau, Y. Du, B. Burchfiel, R. Tedrake, and S. Song. Diffusion policy: Visuomotor policy learning via action diffusion. The International Journal of Robotics Research, page 02783649241273668, 2023.
- [26] K. He, X. Zhang, S. Ren, and J. Sun. Deep residual learning for image recognition. In Proceedings of the IEEE conference on computer vision and pattern recognition, pages 770–778, 2016.

A Details on Dataset Construction

A.1 Dataset Details

Our collected pre-training dataset consists of five categories of paired plugs and sockets: USB connectors, Apple chargers, MicroUSB 3.0, Plugs, and round objects. The complete dataset includes approximately 210,000 data points collected over 5 hours of operational recordings. The hybrid dataset consists of 80% of automated collected data and 20% of manually collected data, which offers good coverage of the workspace with high safety and efficiency.

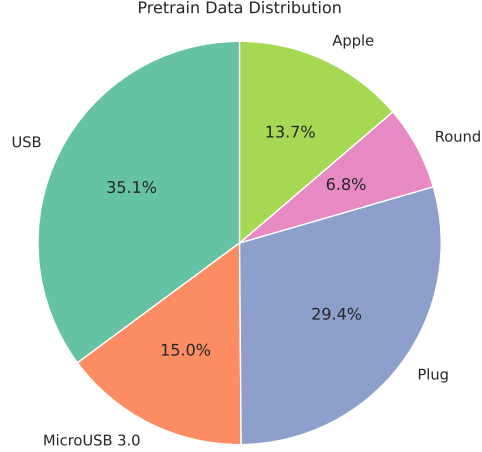


Figure 7: Visualization of pretrain data distribution

A.2 Delta Pose Calculation

When collecting data in a specific environment, we rigidly fix the socket to the table. The data collection workspace is defined as a bounded region of 6 cm in the xy-plane and 10 cm along the z-axis, with rotational constraints of 50 degrees around the socket’s center.

Following InsertioNet [6], we initialize data collection by positioning the Franka gripper where the plug is inserted in the socket. This reference pose is recorded as \mathbf{P}_r . Subsequently, the gripper is moved randomly within the predefined workspace around the socket. We represent the system state at timestep x as $(O_1(x), O_2(x), \mathbf{p}(x))$, where $O_1(x)$ and $O_2(x)$ are the two images captured at time x , and $\mathbf{p}(x)$ denotes the gripper’s pose at time x . The relative pose transformation $\Delta \mathbf{p}$ at time x is then computed as $\mathbf{P}_r \ominus \mathbf{p}(x)$, generating training sample $(O_1(x), O_2(x), \mathbf{P}_r \ominus \mathbf{p}(x))$, where \ominus refers to calculating relative transformation between two pose.

B Details of Model Training

Given dataset $\mathcal{D} = \{(O_1^i, O_2^i, \Delta \mathbf{p}^i)\}_{i=1}^N$, we adopt Diffusion Policy[25] to train a delta-pose prediction model. We adopt the Diffusion Policy [25] as our learning framework. First, a shared ResNet18[26] pretrained on ImageNet is employed as the encoder \mathcal{F} to encode RGB images $O_1, O_2 \in \mathbb{R}^{3 \times 320 \times 320}$ captured by two wrist cameras into visual features v_1, v_2 . We then fuse them together through element-wise addition as $v = v_1 + v_2$. Then, we feed v into the diffusion action head to obtain the delta-pose. The Diffusion Policy formulates action generation as a conditional denoising process. Specifically, starting from a Gaussian noise Δp^K , the denoising network ϵ_θ

performs a K -step denoising procedure to gradually refine the random noise into an action output Δp^0 :

$$\Delta p^{k-1} = \alpha_k (\Delta p^k - \gamma_k \epsilon_\theta(\Delta p^k, k, v)) + \sigma_k \mathcal{N}(0, I) \quad (2)$$

where $\mathcal{N}(0, I)$ represents Gaussian noise, and $\alpha_k, \gamma_k, \sigma_k$ are coefficients determined by the noise scheduler as functions of step k . To train the denoising network ϵ_θ , we randomly sample an action Δa^0 from the training dataset. For each sample, we randomly select a denoising step k and generate the corresponding Gaussian noise ϵ^k . The training objective is formulated as:

$$\mathcal{L} = \text{MSE}(\epsilon^k, \epsilon_\theta(\Delta p^0 + \epsilon^k, k, v)) \quad (3)$$

To enable real-time inference, we adopt DDIM (Denoising Diffusion Implicit Models) as our sampling accelerator, which significantly reduces the number of required denoising steps. Furthermore, to improve the model’s robustness against real-world color variations, we employ strong color augmentation strategies during training, including color jittering and random grayscale conversion. The effectiveness of these augmentation techniques is quantitatively demonstrated through ablation studies in the experimental section.

C Evaluation Environments

We visualize all evaluation environments. During evaluation, we randomly place distraction objects around the socket. We place the socket randomly on the workspace, while maintaining plug and socket’s initial pose deviation in range of $3 \sim 6$ cm in XY transition and $15 \sim 40$ degrees in yaw.

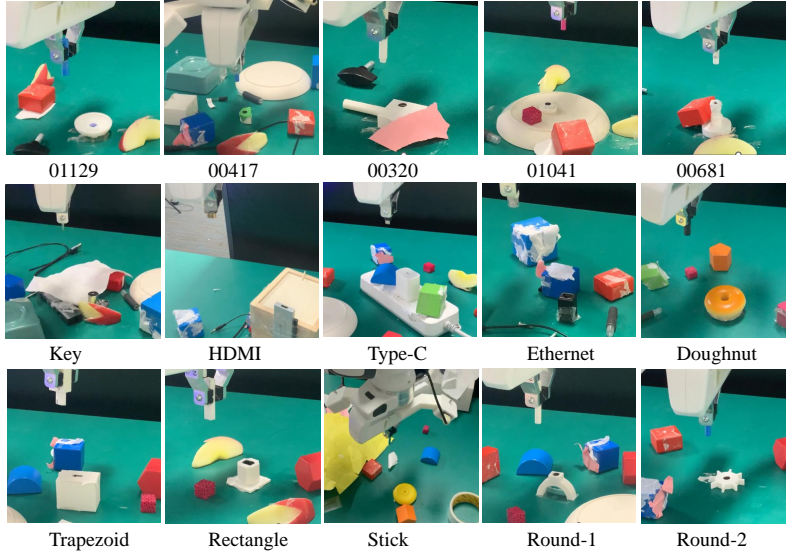


Figure 8: Visualization of real-world evaluation environments.

D Test Object Display

We here visualize all test objects. These test objects are unseen during training with various different colors, shapes and sizes.

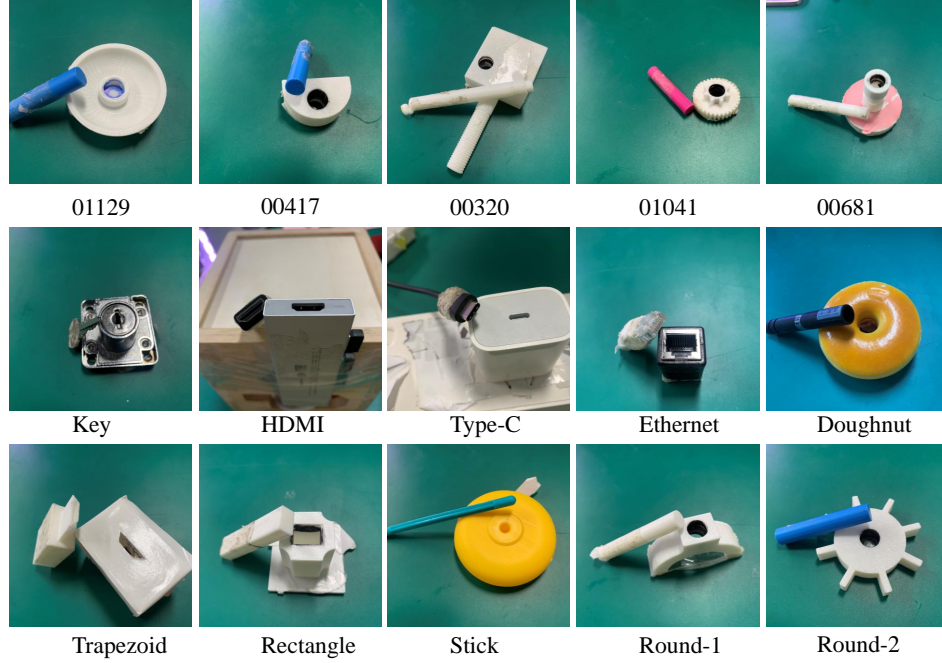


Figure 9: Visualization of unseen test objects.

E Train Object Display

In this section, we visualize all the training objects used in our study. EasyInsert is trained on five categories of common objects, including:

- 8 pairs of USB connectors
- 4 pairs of plugs
- 6 pairs of round objects
- 1 MicroUSB 3.0 connector
- 1 Apple charger

Notably, all selected objects are everyday items that can be easily obtained in household or laboratory environments.



Figure 10: Visualization of training objects.

F Video Snaps of EasyInsert

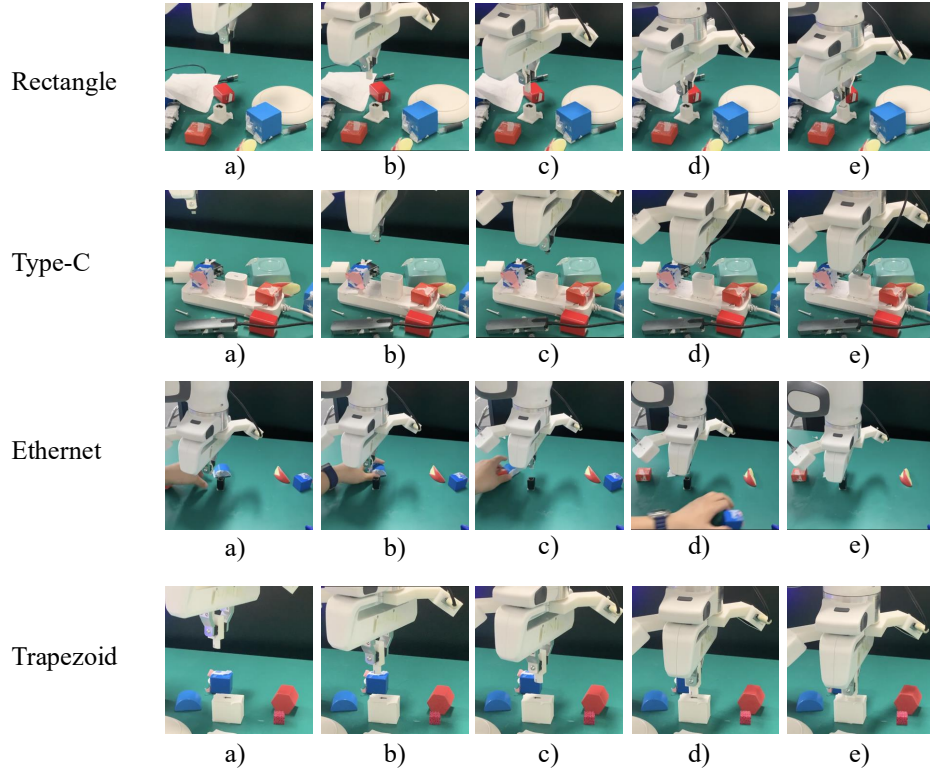


Figure 11: Video snaps of inserting rectangle, Type-C, Ethernet and trapezoid plugs using EasyInsert. We note that during evaluation, we place random distraction objects around the socket. In third row during perturbation experiments, we randomly move socket position and surrounding objects to examine the robustness of EasyInsert. As demonstrated in the video clips, EasyInsert achieves successful zero-shot insertion even in cluttered environments and with large initial pose deviations.

G Failure Case Analysis

As illustrated in Figure 12, we observe that when trained without manual data, while EasyInsert generally succeeds in both the coarse-alignment and fine-adjustment phases, it sometimes fails during the final close-contact phase. This phenomenon underscores the importance of incorporating sufficient manually collected close-proximity data to improve EasyInsert’s performance in the critical close-contact phase.

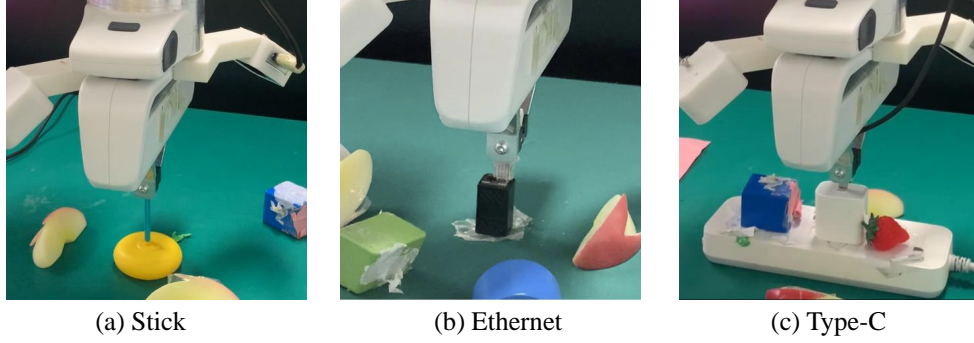


Figure 12: Visualization of failure cases without manual data.